The mandible of *Compsodon helmoedi* (Therapsida: Anomodontia), with new records from the Ruhuhu Basin, Tanzania

Kenneth D. Angielczyk[1,2*] [§], Brandon R. Peecook[3,4] & Roger M.H. Smith[2,5]

[1]*Negaunee Integrative Research Center, Field Museum of Natural History, 1400 South DuSable Lake Shore Drive, Chicago, Illinois 60605, U.S.A.*
[2]*Evolutionary Studies Institute, University of the Witwatersrand, Private Bag 3, WITS, Johannesburg, 2050 South Africa*
[3]*Idaho Museum of Natural History, Idaho State University, 698 E Dillon Street, Pocatello, Idaho 83209, U.S.A.*
[4]*Department of Biological Sciences, Idaho State University, 921 S 8th Ave, Pocatello, Idaho 83209, U.S.A.*
[5]*Karoo Palaeontology, Iziko South African Museum, P.O. Box 61, Cape Town, 8000 South Africa*

Received 21 September 2022. Accepted 13 March 2023

The emydopoid dicynodont *Compsodon helmoedi* originally was named from a single skull collected in *Daptocephalus* Assemblage Zone strata in the South African Karoo Basin. Recently described specimens from the Luangwa Basin, Zambia, have elucidated the species' cranial morphology and facilitated identification of other historical Karoo specimens. Neither the holotype nor any of the described Zambian specimens preserve a mandible; a referred Karoo specimen preserves a highly damaged mandible, but poor preservation obscures most details. We present an additional Zambian *Compsodon* specimen that includes an articulated cranium and mandible, and use μCT data to describe the mandible of this taxon for the first time. The mandible has an upturned dentary symphysis; 'postcanine' teeth with coarse distal denticles; a shallow, elongate posterior dentary sulcus with medial expansion anterior to the tooth row, and a prominent lateral dentary shelf. Although the mandible is similar to those of *Emydops* and *Pristerodon*, it can be differentiated from *Emydops* by the latter's more triangular posterior dentary sulcus, and the absence of a rugose muscle scar on the lateral edge of the lateral dentary shelf. It differs from *Pristerodon* in the absence of a dentary table rostral to the tooth row, the presence of a transverse ridge dividing the lateral dentary shelf into posterior and anterior sections, and the anterodorsal angulation of the lateral dentary shelf. Three fragmentary specimens from the Usili Formation (Ruhuhu Basin) display the same morphotype and represent the first record of *Compsodon* from Tanzania. The expanding geographic range of *Compsodon* underscores its potential as a biostratigraphic index fossil, but more information on its stratigraphic and temporal ranges is needed to realize that potential.

Keywords: Synapsida, Dicynodontia, Emydopoidea, Permian, Tanzania, Zambia.

INTRODUCTION

Compsodon helmoedi van Hoepen, 1934 is one of numerous dicynodonts that were described from the Karoo Basin of South Africa in the first half of the 20th century and subsequently languished in obscurity because of the taxonomic problems that long plagued the group. Recent studies of many of these taxa have shown that some are indeed valid, and in other cases clarified synonymies among them (e.g. Kammerer *et al*. 2011; Angielczyk & Rubidge 2013; Kammerer *et al*. 2015a,b; Angielczyk *et al*. 2016). As part of this work, Angielczyk & Kammerer (2017) confirmed that *C. helmoedi* is a valid species with diagnostic autapomorphies, and also described new specimens that extended its geographic range to the Luangwa Basin of Zambia. However, our knowledge of the anatomy of *C. helmoedi* is still limited, because the holotype and the newly referred Zambian specimens only consist of isolated crania. One historical specimen from the Karoo Basin (RC 736; Fig. 1a) consists of a skull with an articulated mandible, but the specimen is poorly preserved and prepared, and it provides little information about the morphology of the mandible aside from confirming the presence of a mandibular fenestra (although this character is useful for differentiating *Compsodon* from *Dicynodontoides*; Angielczyk & Kammerer 2017).

Recent preparation of a small dicynodont specimen (NHCC LB211; Fig. 1B–D) that was collected in the Luangwa Basin in 2009 has revealed a partial skeleton of *C. helmoedi*, including a well-preserved, articulated cranium and mandible. Here we describe the mandible of NHCC LB211 and discuss its implications for our understanding of the phylogeny of emydopoid dicynodonts. Furthermore, the new anatomical information provided by NHCC LB211 has allowed us to identify three isolated mandibles from the Ruhuhu Basin, Tanzania, as also belonging to *C. helmoedi*. These new records expand the geographic range of the species and underscore its potential utility as a late Permian index fossil in southern and eastern Africa.

*Author for correspondence. E-mail: kangielczyk@fieldmuseum.org

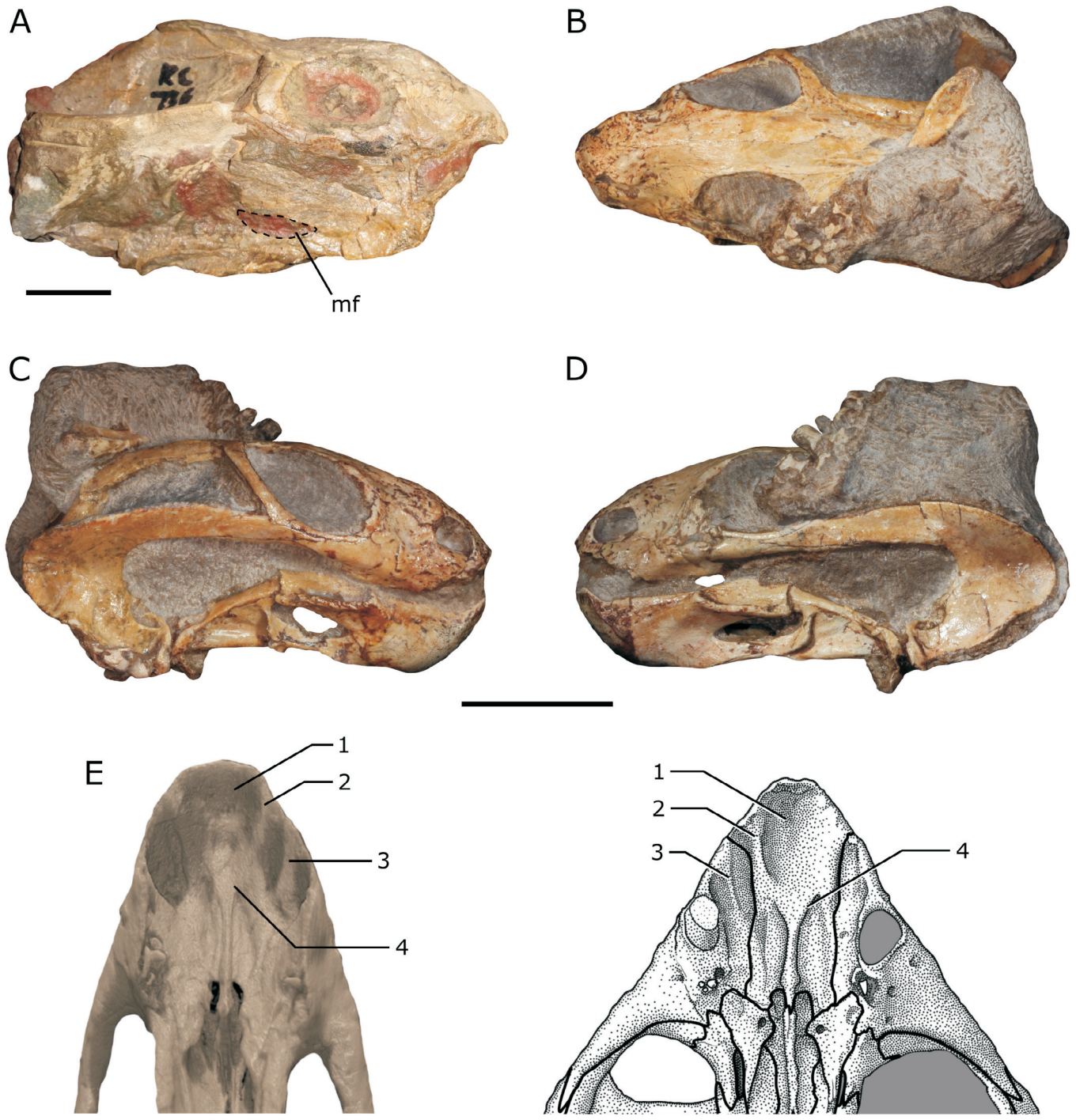

Figure 1. South African specimen of *Compsodon helmoedi* (RC 736) that preserves a mandible (**A**) (photo by C. Kammerer). Zambian specimen of *C. helmoedi* (NHCC LB211) that preserves a mandible in dorsal (**B**), right lateral (**C**), and left lateral (**D**) views. (**E**) μCT rendering of the anterior palate of NHCC LB211 (left) and interpretive drawing of the anterior palate of NHCC LB14 (right; modified from Angielczyk & Kammerer 2017) showing the autapomorphic secondary palate morphology of *C. helmoedi*. Both specimens possess an anterior median depression (1), lateral anterior palatal ridges (2), an embayment of the palatal rim anterior to the caniniform process divided into two depressions by a posteromedially-trending ridge (3), and a Y-shaped anterior end of the posterior median palatal ridge (4). Scale bars are 2 cm. The upper scale bar applies to panel A; the lower scale bar applies to panels B–D. The images in E are not to scale. Abbreviations: mf, mandibular fenestra.

SYSTEMATIC PALAEONTOLOGY

Therapsida Broom, 1905
Anomodontia Owen, 1860
Dicynodontia Owen, 1859
Therochelonia Seeley, 1894
Emydopoidea van Hoepen, 1934

Compsodon helmoedi van Hoepen, 1934

Holotype. NMQR 1460: a nearly complete, laterally compressed skull (Angielczyk & Kammerer 2017).

Newly referred material. NHCC LB211: partial skeleton including articulated cranium and mandible; vertebrae; ribs; articulated right scapulocoracoid; right clavicle; partial left and right humeri; articulated ?left radius, ulna, and partial manus; ?right radius; partial articulated ?right manus; articulated right innominate; partial femur. NMT

RB1100, NMT RB1136, NMT RB1254: three isolated partial mandibles.

Revised diagnosis. Angielczyk & Kammerer (2017) provided a detailed diagnosis of *C. helmoedi* based on cranial morphology. To that diagnosis, we add the following characters of the mandible: dentary symphysis shovel-shaped, with a broad, shallow fossa on its posterodorsal surface; dentary table absent; posterior dentary sulcus present with a rounded medial expansion at its anterior end; four to seven laterally compressed dentary teeth with coarse denticles on their lingual edges; lateral dentary shelf prominent with a transverse ridge on the widest point of the dorsal surface; oval fossa present near the posterior end of the lateral surface of the lateral dentary shelf; external mandibular fenestra open laterally and not occluded by a lamina of the dentary.

Locality and horizon. NHCC LB211 was collected at locality L35, near the southern end of North Luangwa National Park, Luangwa Basin, Zambia. L35 falls in the Lopingian (upper Permian) Upper Madumabisa Mudstone Formation, specifically in 'lithofacies association 2' of Sidor *et al*. (2021). The mudrock-dominated lithofacies association 2 is peculiar from a palaeoenvironmental perspective relative to more consistently fluvial sediments lower in section, being a distal floodplain setting with evidence of desiccation and loessic dust deposition. It also preserves the younger assemblage, including all Zambian *C. helmoedi*, of a putative two-part subdivision of the Upper Madumabisa Mudstone Formation fauna currently under study (Peecook *et al*. 2020).

NMT RB100 and RB1136 were collected at locality Z04, which is located about 1.5 km southeast of Chingole (Kingori) Mountain, Ruhuhu Basin, Tanzania. Stratigraphically, this locality falls in the upper portion of the Middle Grey Mudrock (Kaaya 1992) of the Lopingian Usili Formation. NMT RB1254 was collected at locality Z244, which is located about 600 m southeast of Z04. Z244 is stratigraphically higher than Z04, falling in the Upper Pebbly Sandstone (Kaaya 1992) of the Usili Formation. Detailed locality information is available on request to qualified researchers from the National Heritage Conservation Commission (Luangwa Basin specimen), the National Museum of Tanzania (Ruhuhu Basin specimens), or the authors.

METHODS

NHCC LB211 underwent x-ray μCT-scanning at the University of Chicago PaleoCT facility using a GE v|tome|x s 240 scanner. Data were acquired using an acceleration voltage of 190 kV, an e-beam current of 200 μA, and a 0.1 mm tin filter. The scan resulted in a stack of 1891 images, and the reconstructed volume has an isotropic voxel size of 40.46 μm. CT scan data are available on request from the NHCC or the Field Museum of Natural History. Segmentation of the specimen was carried out in ORS Dragonfly version 2021.1.

The phylogenetic position of *Compsodon helmoedi* as the sister taxon of *Emydops* spp. has remained stable following the redescription of the taxon by Angielczyk & Kammerer (2017) (e.g. Kammerer 2019; Angielczyk *et al*. 2019; Olivier *et al*. 2019; Liu 2020; Kammerer & Ordoñez 2021). To test whether the addition of mandibular characters for *C. helmoedi* would change the level of support for this relationship, we coded a total of 29 additional characters (26 discrete-state, 3 continuous) related to the mandible and lower dentition for *C. helmoedi* in the phylogenetic dataset of Angielczyk *et al*. (2021). These comprise all the characters related to mandible and lower dentition except one that was previously coded based on RC 736, and two related to the reflected lamina of the angular that could not be coded because the lamina is not preserved in any of the available specimens. We also corrected an incorrect coding for one character (discrete state character 109; previously coded as state 0, but recoded as state 1). Finally, we split the previous genus-level coding for *Emydops* into two species-level operational taxonomic units (OTUs), *E. arctatus* and *E. oweni*. Our coding for *E. oweni* is based on the three specimens referred to this species by Fröbisch & Reisz (2008) (BP/1/2626, SAM-PK-3721, SAM-PK-10172); the coding for *E. arctatus* was based on all remaining reference specimens used for *Emydops* in the Angielczyk *et al*. (2021) dataset and previous iterations of the data matrix.

The final dataset included 115 OTUs and 197 characters, of which 174 are discrete binary or multistate characters (seven ordered, 167 unordered). All discrete-state characters were weighted equally. The remaining 23 characters are continuous. We treated the continuous characters as additive using the method of Goloboff *et al*. (2006), with mean values used as the codings for the OTUs except in cases when only a single measurement was available for an OTU. Unknown and inapplicable discrete state and continuous characters were coded as '?' (Strong & Lipscomb 2000).

We conducted a parsimony analysis of the dataset using TNT 1.6 (December 2022 version) (Goloboff *et al*. 2008; Goloboff & Catalano 2016; Goloboff & Morales 2023), using two tree search strategies. The first search used the new technology methods of TNT, specifically a driven search with the initial search level set at 65, which was checked every five hits. The initial number of addition sequence replicates was 1000, and the search was required to find the shortest length trees 20 times. The analysis started with default settings for sectorial searching, tree drifting, parsimony ratchet and tree fusing. The second analysis utilized the traditional search method of TBR branch swapping with 10 000 replicates and 10 trees held per replicate. *Biarmosuchus* was the outgroup for both analyses.

We utilized symmetric resampling (Goloboff *et al*. 2003), jackknife analysis (Mueller & Ayala 1982; Farris *et al*. 1996) and decay analysis (Bremer 1988, 1994) to measure support for the most parsimonious cladograms. The symmetric resampling results are based on 10 000 replicates with a change probability of 33%. Each replicate included a new technology search with default settings for tree drifting, parsimony ratchet and tree fusing, and 10 random addition sequence replicates. Absolute frequency values were used to summarize the results (Kopuchian & Ramírez 2010). For the jackknife analysis of clade

support we utilized 10 000 resampling replicates, with a 36% probability of character removal, and the same search parameters as the symmetric resampling analysis. The decay analysis results are based on a sample of suboptimal cladograms with lengths up to six steps longer than the most parsimonious cladograms. Following the recommendations of Goloboff *et al*. (2008), the suboptimal trees were generated through a series of traditional searches in which the length and number of suboptimal cladograms retained were both incrementally increased. The resulting cladograms were filtered to remove duplicates, so all 882,503 cladograms in the sample are unique.

IDENTIFICATION OF NHCC LB211

It is critical to establish the taxonomic identity of NHCC LB211 to ensure that its mandibular morphology pertains to *C. helmoedi* and not another taxon. Angielczyk & Kammerer (2017) noted that *C. helmoedi* is diagnosed by an autapomorphic morphology of the secondary palate, including the following characters: median depression at the anterior end of the premaxillary secondary palate; medial anterior palatal ridges absent, but lateral anterior palatal ridges prominent and extend to posterior end of secondary palate; Y-shaped anterior end of the posterior median palatal ridge; embayment of the palatal rim anterior to the caniniform process divided into two depressions by a posteromedially-trending ridge (Fig. 1E). The articulated mandible of NHCC LB211 obscures the secondary palate, but examination of the μCT data reveals that the specimen possesses each of the characters listed above (Fig. 1E). A number of the other features noted in Angielczyk & Kammerer's (2017) diagnosis are also visible externally or in the μCT data, including: a diamond-shaped nasal boss with a continuous posterior margin; posterior portion of the frontals depressed, giving the postfrontals a raised appearance; presence of a postcaniniform keel on the maxilla; presence of a small number of maxillary teeth with conical, unserrated crowns; groove on the ventral surface of the mid-ventral vomerine plate, anterior pterygoid rami with straight lateral edges; and presence of a tall, blade-like crista oesophagea with a shallow groove on its anterior surface (Figs 1B–E, 2C). Some characters of NHCC LB211 that differ from the diagnosis of *C. helmoedi*, such as the very weak development of the lip-like eminences of the parietals surrounding the pineal foramen, may stem from the small size of the specimen (basal skull length 54.2 mm compared to the maximum of 112 mm reported by Angielczyk & Kammerer [2017]), although Olroyd *et al*. (2021) noted that fusion of the braincase elements indicated that it was unlikely to represent an early-stage juvenile. It may represent a late-stage juvenile or subadult instead. Given the close correspondence between the diagnosis of *C. helmoedi* and the morphology of NHCC LB211, we are confident in its referral to the species, and in its use as a source of information about parts of the skeleton that are not preserved in previously described specimens.

THE MANDIBLE OF NHCC LB211

The mandible of NHCC LB211 is preserved in articulation with the skull. Its lateral, ventral, and medial surfaces have been almost completely exposed via mechanical preparation, but the dorsal surface remains obscured and has been visualized using the μCT data.

The left and right dentaries are fused into a single element, with no sign of a suture visible externally or in the μCT data (Fig. 2). The anterior face of the dentary is smoothly rounded and lacks a longitudinal median ridge. Numerous small vascular foramina, and more scattered larger foramina, cover the anterior surface of the dentary and extend onto its lateral sides back to the level of the anterior margin of the lateral dentary shelf. The dorsal edge of the symphysis projects above the dentary rami and is anterodorsally angled. The symphysis is shovel-shaped (see discussion of this character in Angielczyk [2001]), with a broad, shallow fossa on its posterior surface, but is shorter and broader than the elongate, tapering symphysis of *Dicynodontoides* (Cox 1959).

A dentary table is absent. Instead, the dorsal surface of the dentary immediately posterior to the symphysis forms a narrow, rounded edge (Fig. 2D). Farther posteriorly, a shallow, wide posterior dentary sulcus (*sensu* Angielczyk & Rubidge 2013) is present, which extends slightly posterior to the dentary tooth row. The sulcus narrows anteriorly, but bears a small, curved, medial expansion at its anterior end that extends slightly anterior to the first tooth position. The margins of the posterior dentary sulcus are low and rounded, and are unlike the taller, blade-like lateral or medial edges found in some cistecephalids (Cluver 1974; Angielczyk *et al*. 2019).

A prominent lateral dentary shelf is present, which can be divided into two subsections (Fig. 2). The more posterior subsection overhangs the external mandibular fenestra, and its lateral edge bears a shallow posterolateral fossa at its posterior end (Fig. 2A,B), similar to that observed in *Kombuisia* (Fröbisch 2007; Fröbisch *et al*. 2010). When the dorsal surface of the dentary ramus is held horizontally, the posterior subsection is angled anterodorsally such that its anterior end approaches the dorsal margin of the dentary. In dorsal view (Fig. 2D), the posterior subsection is of a constant mediolateral width for most of its length, but narrows near its posterior end. A shallow fossa occupies the dorsal surface of the posterior subsection. Just anterior to this fossa a strong, rounded transverse ridge separates the posterior subsection of the lateral dentary shelf from the anterior subsection (Fig. 2D), and marks the closest approach of the lateral dentary shelf to the dorsal surface of the dentary. The lateral edge of the anterior subsection is angled anteromedially, giving the subsection a triangular shape in dorsal view, and its dorsal surface is slightly convex. The anterior subsection extends forward to the level of the first tooth position. In lateral view, the anterior subsection angles anteroventrally such that its anterior tip is at about the same height as the posterior end of the lateral dentary shelf. The lateral dentary shelf lacks the prominent, rugose muscle scar found in *Emydops* (Angielczyk *et al*. 2005; Fröbisch & Reisz 2008).

Below the lateral dentary shelf, the dentary forms the anterior margin of the external mandibular fenestra on

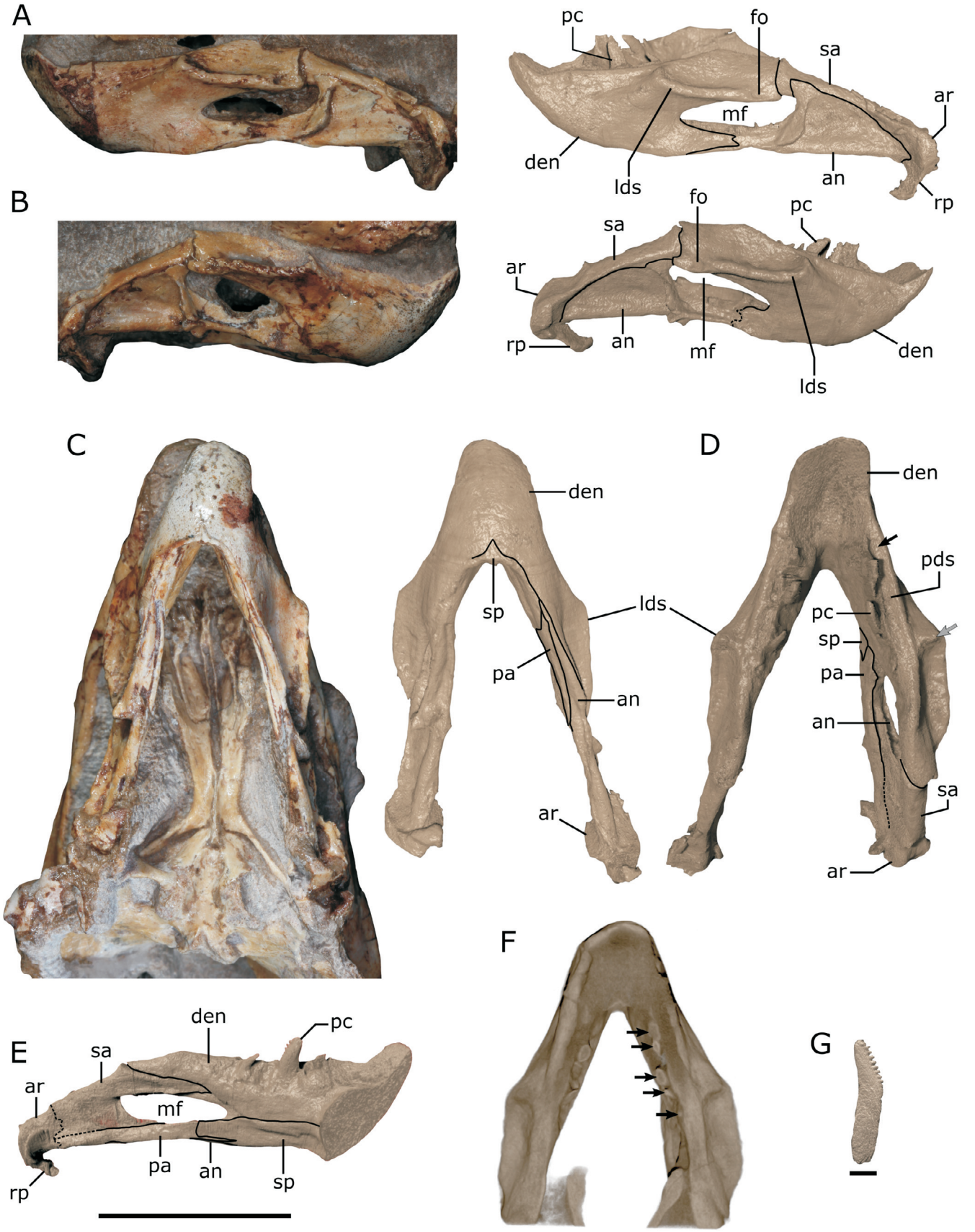

Figure 2. The mandible and lower teeth of *Compsodon helmoedi*. Photograph and μCT rendering of NHCC LB211 in left lateral (**A**), right lateral (**B**), and ventral (**C**) views. μCT rendering of the mandible of NHCC LB211 in dorsal view (**D**). μCT rendering of the left mandibular ramus of NHCC LB211 in medial view (**E**). μCT horizontal section through the dorsal surface of NHCC LB211 in dorsal view (**F**). μCT rendering of a right mandibular tooth in lingual view (**G**). The black arrow in D highlights the medial expansion of the posterior dentary sulcus; the gray arrow highlights the transverse ridge on the dorsal surface of the lateral dentary shelf. The black arrows in F highlight portions of five functional teeth that are visible in the plane of the horizontal section. Lower left scale bar is 2 cm and applies to panels A–F. Lower right scale bar is 5 mm and applies to panel G. Abbreviations: an, angular; ar, articular; den, dentary; fo, fossa; lds, lateral dentary shelf; mf, mandibular fenestra; pa, prearticular; pc, 'postcanine' tooth; pds, posterior dentary sulcus; rp, retroarticular process; sa, surangular; sp, splenial.

the lateral surface of the mandible, as well as most of the dorsal margin and about half of the ventral margin (Fig. 2A,B). Posteriorly, an anterior process of the surangular slots into the rear of the dentary and extends anteriorly to close to the posterior end of the tooth row. The dentary surrounds the lateral, dorsal, and medial surfaces of the surangular anterior process, and the CT data show that the interior surfaces of the elements are smooth and separated by a small gap that suggests the presence of a soft tissue connection in life. On the lateral surface of the mandible, the external manifestation of this joint is a vertical contact at the posterior end of the dentary, but on the medial side it has the form of a long, anteroventrally-sloping scarf joint (Fig. 2E). Ventral to the mandibular fenestra the dentary forms a tapering posterior process that rests in a depression on the lateral surface of the angular.

The tooth row begins at the level of the posterior margin of the dentary symphysis and extends posteriorly to about the level of the midpoint of the lateral dentary shelf (Fig. 2D,F), and at least six functional teeth are present (Olroyd *et al*. 2021). As is typical of most dicynodonts, the tooth row is positioned toward the medial side of the dentary, and is bounded laterally by the posterior dentary sulcus. The dentary teeth are relatively large, with somewhat laterally compressed, blade-like crowns that bear coarse distal denticles (Fig. 2G), similar to the dentary teeth of many other toothed dicynodonts (e.g. Angielczyk *et al*. 2014a). However, this morphology contrasts with the smaller, conical, unserrated crowns of the maxillary 'postcanines' (Fig. 1E; also see Angielczyk & Kammerer 2017). The μCT data reveal replacement teeth at some tooth positions in the mandible, which form medially to the functional teeth. Additional information on tooth replacement in NHCC LB211 can be found in Olroyd *et al*. (2021).

The splenial is a fused, single element, with no midline suture visible. Anteriorly, it contributes to the ventral and posterior surfaces of the symphysis (Fig. 2C,E). The μCT data reveal that the splenial projects forward into a depression on the dentary, and that an internal cavity bounded by the splenial and dentary is present within the symphysis, similar to that described for *Kembawacela* (Angielczyk *et al*. 2019). In ventral view, the symphyseal portion of the splenial bears a pointed, triangular process that projects a short distance onto the anterior face of the symphysis (Fig. 2C). Near the ventral margin of the posterior symphyseal surface, a weak midline ridge separates two shallow fossae. Farther posteriorly, the splenial bears a pair of plate-like processes that contribute to the medial surfaces of the mandibular rami (Fig. 2E). Close to the symphysis the posterior process of the splenial is in contact with the medial surface of the dentary, but farther along the ramus an anterior process of the angular wedges between the splenial and the dentary. At its posterior end, the posterior process of the splenial bifurcates and the anterior end of the prearticular slots into the resulting recess, forming a scarf joint.

The surangular forms the dorsal portion of the postdentary region of the mandible (Fig. 2). Anteriorly, it slots into a groove on the underside of the dentary, and extends forward to about the level of the posterior end of the tooth row. This anterior process tapers anteriorly and is not visible on the lateral surface of the mandible, but much of it is exposed on the medial surface below the anteroventrally sloping contact with the dentary (Fig. 2E). Near the junction with the dentary, the surangular makes a small contribution to the dorsal and posterior margins of the external mandibular fenestra (Fig. 2A,B) and more extensive contributions to these parts of the internal mandibular fenestra (Fig. 2E). Posterior to the dentary, the surangular is broadest dorsally, forming the transversely expanded dorsal margin of the mandible (Fig. 2D). Below the expanded dorsal edge, the surangular rapidly narrows to a thin plate, which forms much of the postdentary region. The lateral surface of this plate is overlapped by a thin lamina of the angular, but the plate is well exposed on the medial surface of the mandible (Fig. 2E). The prearticular overlaps the ventral portion of the medial surface of the plate. Posteriorly, the surangular contacts the articular, but the details of this joint are not easy to discern on the physical specimen or in the μCT data.

The angular is a complexly-shaped bone that forms much of the lateral and ventral surfaces of the postdentary region of the mandible (Fig. 2). Anteriorly, the angular forms a thin, laterally compressed process that wedges between the dentary and the splenial. In ventral view this anterior process extends to about the level of the midpoint of the lateral dentary shelf (Fig. 2C), but the CT data reveal that it continues internally to the level of the anterior end of the lateral dentary shelf. Moving posteriorly, the angular takes on a thicker, subtriangular cross-section, and bears a vertical lamina on its lateral side. The lateral surface of this lamina forms a triangular fossa (apex directed posteriorly) in which the posterior process of the dentary rests (Fig. 2A). Beginning at about the mid-length of the mandibular fenestra, the angular is exposed on the lateral surface of the mandible, and it contributes to the ventral and posterior borders of the external mandibular fenestra (Fig 2A,B). Posterior to the mandibular fenestra, the angular consists of a slightly thickened ventral portion that rapidly narrows dorsally to form an extremely thin lamina that overlaps the lateral surfaces of the surangular and the articular. The ventral portion of the angular has a small exposure on the medial surface of the mandible, where it is overlapped by the prearticular. A thickened vertical ridge immediately behind the mandibular fenestra marks the base of the reflected lamina of the angular, but the reflected lamina itself is not preserved on either side of the mandible (Fig 2A,B).

The thin, strap-like prearticular extends along the medial surface of the mandible between the articular and the splenial (Fig. 2). Its posterior contact with the articular is indistinct, but its anterior end slots into the posterior side of the splenial (Fig. 2C,E). The lateral side of the prearticular is in contact with the angular and surangular, and although it is located toward the ventral margin of the medial surface of the mandible, the prearticular is not exposed on the lateral side of the mandible.

Neither articular is completely exposed in NHCC LB211,

but the μCT data indicate that the right articular is somewhat better preserved than the left (Fig. 2). As is typical of dicynodonts, the articular surface for the quadrate consists of two dorsally convex, anteroposteriorly elongate surfaces separated by a rounded median ridge. The lateral articular surface is anteroposteriorly longer than the medial, and its lateral edge is somewhat thickened. This thickened edge is continuous with the transversely expanded dorsal portion of the surangular (Fig. 2A,B), but the lateral articular surface itself is separated from the dorsal edge of the surangular by a shallow articular recess (*sensu* Crompton & Hotton 1967). The medial articular surface is quite thin in the dorsoventral dimension, and is offset slightly ventrally relative to the lateral surface (Fig. 2D,E). It is also anteroposteriorly shorter and mediolaterally narrower than the lateral one, and curves dorsomedially. The retroarticular process is long and triangular in cross-section, with the apex of the triangle pointing laterally. The process projects anteroventrally from the ventral surface of the articular (Fig. 2A,B); this morphology is more pronounced on the right side than the left, and the left side may better represent the original morphology. Although the retroarticular process joins with the thickened lateral edge of the articular proximally, it is well-separated from the articular surfaces, in contrast to many other dicynodonts in which the process is nearly continuous with the articular surfaces. The distal end of the process is transversely expanded compared to its shaft. Anteriorly, the articular contacts the angular, the surangular, and the prearticular (Fig. 2E), but the sutures between these elements are indistinct.

COMPARISON

Compsodon helmoedi has been documented in strata referred to the *Dicynodon-Theriognathus* Subzone of the *Daptocephalus* Assemblage Zone in the Karoo Basin of South Africa and the Upper Madumabisa Mudstone Formation in the Luangwa Basin of Zambia (Angielczyk *et al*. 2014b; Angielczyk & Kammerer 2017; Viglietti 2020). Most of the other dicynodonts known from these strata lack dentary teeth, making their mandibles easy to distinguish from those of *C. helmoedi*. The toothed dicynodont *Endothiodon* also can be differentiated from *C. helmoedi* by the former's larger size, pointed dorsal tip of the dentary symphysis, and expanded bosses on the ventral margin of the dentary, as well as the presence of multiple dentary tooth rows in some individuals (e.g. Cox 1964; Ray 2000; Macungo *et al*. 2020; Olroyd *et al*. 2021). However, two small, toothed dicynodonts that occur in the Karoo and Luangwa Basins, *Pristerodon* and *Emydops*, are comparable in size to *C. helmoedi* and have similar mandibular morphologies. Therefore, it is important to identify diagnostic characters that can be used to differentiate isolated or fragmentary specimens of these taxa in collections or in the field.

Six characters of the dentary distinguish *Pristerodon* from *Compsodon* (Fig. 3). In dorsal view, the posterior dentary sulcus of *Pristerodon* bows laterally near its posterior end and narrows anteriorly (Fig. 3F), whereas that of *Compsodon* is straighter and has a curved medial expansion at its anterior end (Fig. 3E). *Compsodon* also lacks a dentary table (*sensu* Angielczyk & Rubidge 2013) anterior to the posterior dentary sulcus (Fig. 3G), but in *Pristerodon* a shallow, groove-like dentary table is present (Fig. 3F). A prominent lateral dentary shelf that narrows anteriorly is present in both *Pristerodon* and *Compsodon*, but the dorsal surface of the shelf bears a strong transverse ridge at its widest point in *Compsodon* (Fig. 3E), whereas the ridge is absent in *Pristerodon (*Fig. 3F). In lateral view, the posterior portion of the lateral dentary shelf of *Compsodon* is angled dorsally, such that the lateral dentary shelf approaches the dorsal edge of the dentary (Fig. 3A). In *Pristerodon*, the lateral dentary shelf is horizontal and is located lower on the lateral surface of the dentary, such that it does not approach the dorsal edge of the dentary (Fig. 3B). Finally, the lateral edge of the lateral dentary shelf bears a shallow, oval depression near its posterior end in *Compsodon* (Fig. 3a), similar to the depression in this area reported for *Kombuisia* (Fröbisch 2007; Fröbisch *et al*. 2010). *Pristerodon* lacks this depression.

The mandibles of *Emydops* and *Compsodon* are very similar in most respects (Fig. 3), likely reflecting their hypothesized close phylogenetic relationship (Angielczyk & Kammerer 2017). The situation is further complicated by the fact that the two currently-recognized species of *Emydops*, *E. arctatus* and *E. oweni*, differ in some aspects of their mandibular morphology, especially the morphology of the lateral dentary shelf (Fröbisch & Reisz 2008). However, characters of the dentary can be used to differentiate the mandibles of *Compsodon* from *E. arctatus* and *E. oweni*. In dorsal view, the lateral and medial walls of the posterior dentary sulcus are straight but diverge anteriorly in both species of *Emydops*, giving the sulcus a triangular shape (Fig. 3G,H). By contrast, the sulcus in *Compsodon* maintains a near-constant width except for the rounded medial expansion at its anterior end (Fig. 3E). The lateral dentary shelf is large in *Compsodon*, *E. arctatus*, and *E. oweni*, but the dorsal surface of the shelf is convex in *E. oweni* and the ventral surface is concave, causing the shelf to slope ventrolaterally (Fig. 3C) (Fröbisch & Reisz 2008). *Compsodon* is more similar to *E. arctatus* in having a concave dorsal surface of the lateral dentary shelf and a convex ventral surface that together cause the shelf to slope dorsolaterally (Fig. 3A,D). A ridge is present on the dorsal surface of the lateral dentary shelf in *Compsodon* and both *Emydops* species. However, in *Compsodon* the ridge is oriented transversely (Fig. 3E), whereas in *Emydops* the ridge is angled anterolaterally (Fig. 3G,H). In lateral view, a prominent, rugose muscle scar is present at the widest point of the lateral dentary shelf in *Emydops* (Angielczyk *et al*. 2005; Fröbisch & Reisz 2008). This scar forms a fairly distinct, ventrolaterally-oriented projection in *E. oweni* (Fig. 3C), but in *E. arctatus* the scar is somewhat smaller and includes striated texturing on the lateral surface of the lateral dentary shelf (Fig. 3D). In *Compsodon*, the lateral surface of the lateral dentary shelf is smoothly rounded and the muscle scar is absent (Fig. 3A). Finally, the lateral edge of the lateral dentary shelf bears a shallow, oval depression near its posterior end in *Compsodon* (Fig. 3A), but this depression is absent in both species of *Emydops*.

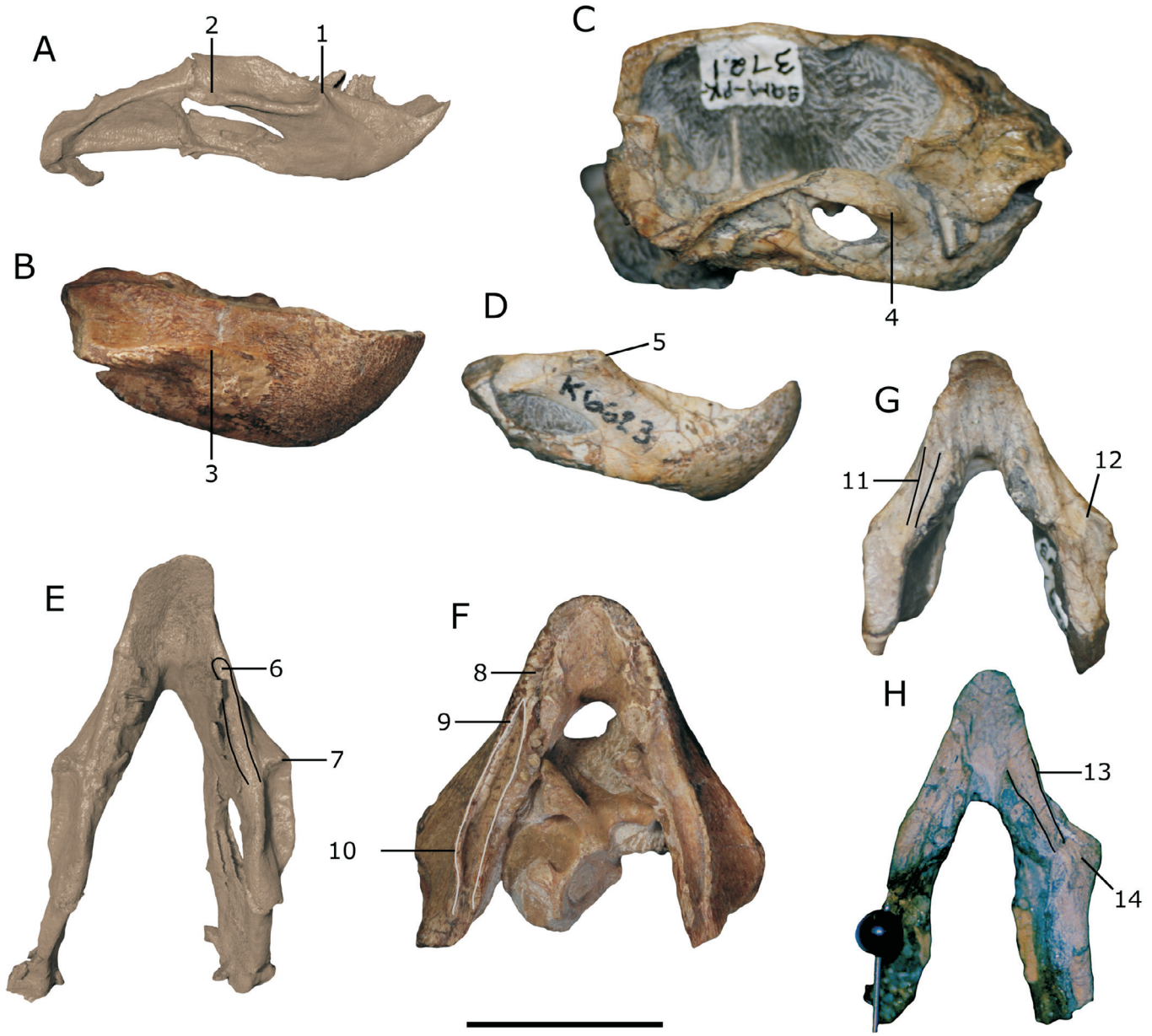

Figure 3. Specimens showing morphological differences between the mandibles of *Compsodon*, *Emydops*, and *Pristerodon*. In lateral view (**A**), the lateral dentary shelf of *Compsodon* (NHCC LB211) closely approaches the dorsal edge of the dentary (1) and bears an oval fossa (2) near its posterior end. In lateral view (**B**), the lateral dentary shelf of *Pristerodon* (NHCC LB190) does not closely approach the dorsal edge of the dentary (3); it also lacks an oval fossa near its posterior end. In lateral view, the lateral dentary shelves of *Emydops oweni* (SAM-PK-3721; **C**) and *E. arctatus* (SAM-PK-K6623; **D**) approach the dorsal edge of the dentary, but bear a prominent, rugose muscle scar on their lateral surfaces (4, 5) and lack an oval fossa near their posterior ends. In dorsal view (**E**), the posterior dentary sulcus of C*ompsodon* (NHCC LB211) displays a medial expansion near its anterior end (6), and a transverse ridge is present on the dorsal surface of the lateral dentary shelf (7). In dorsal view (**F**), the mandible of *Pristerodon* (NHCC LB190) bears a dentary table (8; absent in *Compsodon*), the posterior dentary sulcus narrows anteriorly (9) and bows laterally near its posterior end (10). In dorsal view, the mandibles of *Emydops arctatus* (SAM-PK-K6623; **G**) and *E. oweni* (BP/1/262; **H**) display a triangular dentary sulcus that widens anteriorly (11, 13); the dorsal surfaces of the lateral dentary shelves bear a ridge, but it is angled posteriorly (12, 14). Scale bar is 2 cm.

NEW RECORDS OF *COMPSODON HELMOEDI* FROM TANZANIA

There are no previous reports of *C. helmoedi* from the Ruhuhu Basin of Tanzania (e.g. Gay & Cruickshank 1999; Sidor *et al*. 2010; Angielczyk *et al*. 2014a,b). However, the description of the mandible of NHCC LB211 has allowed us to identify three fragmentary mandibles from the upper Permian Usili Formation as representing the species.

The first of these specimens, NMT RB1100, preserves a nearly complete dentary symphysis, most of the left dentary ramus, part of the right dentary ramus, and a small part of the left ramus of the splenial. Four teeth are preserved in the left ramus, and five are present in the right (Fig. 4B,G). All of the teeth are broken, but the broken surfaces of several of the teeth are teardrop-shaped, consistent with the morphology expected if the crowns were laterally compressed like those of NHCC LB211. A dentary table is absent; instead, the dorsal surface of the dentary ramus immediately posterior to the symphysis comes to a narrow, rounded edge (Fig. 4G). More posteriorly, a shallow posterior dentary sulcus is present, and it has a rounded medial expansion at its anterior end that is very similar to that observed in NHCC LB211 (Fig. 4F,G). Only the anterior half of the left lateral dentary

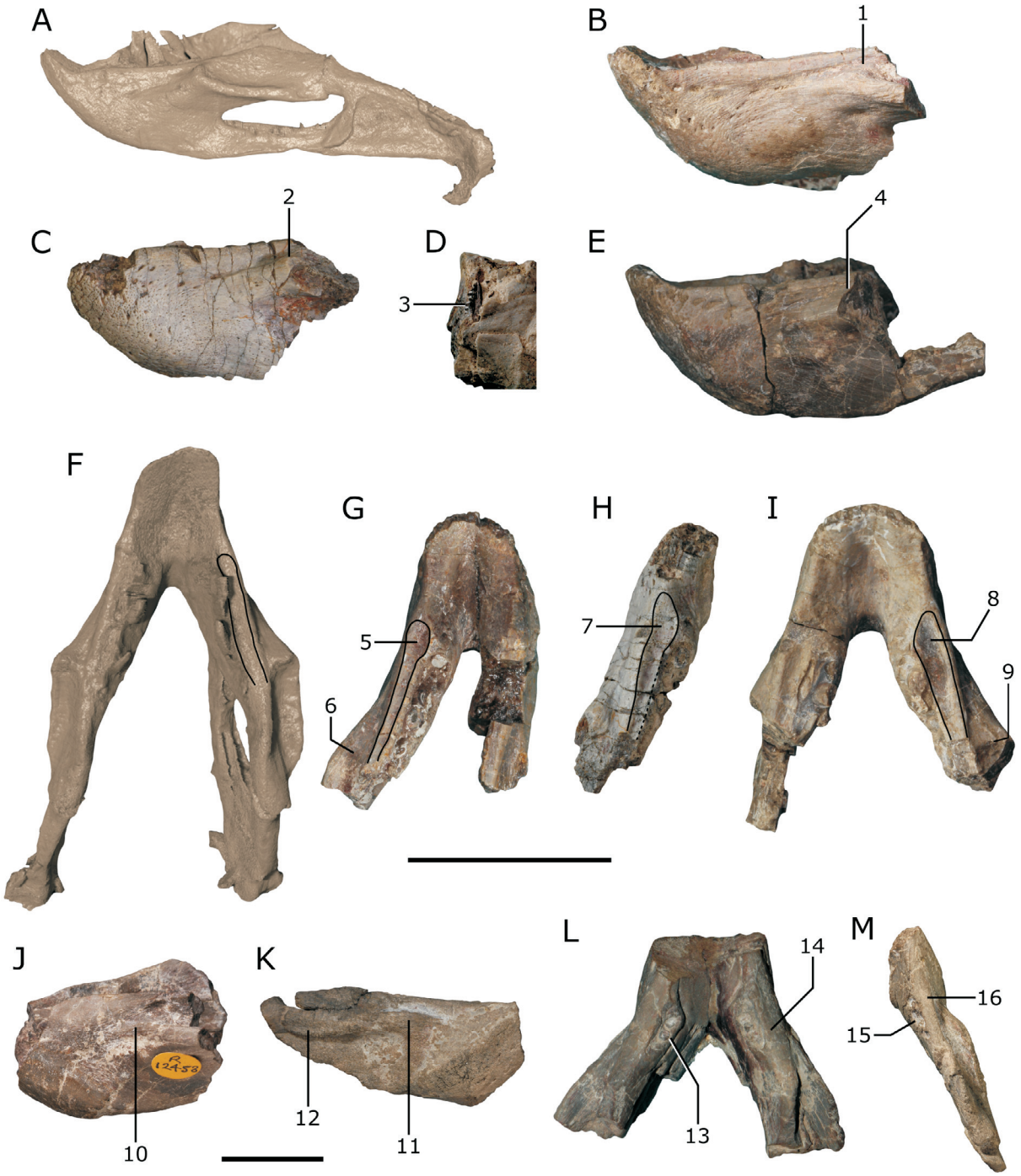

Figure 4. Tanzanian specimens of *Compsodon helmoedi* and similar taxa. **A**, Zambian mandible of *C. helmoedi* (NHCC LB211) in left lateral view for comparison. **B**, Partial dentary of *C. helmoedi* from Tanzania (NMT RB1100) in left lateral view. As in the Zambian specimen, the lateral dentary shelf closely approaches the dorsal edge of the dentary (1) in lateral view. **C**, Partial dentary of *C. helmoedi* from Tanzania (NMT RB1136) in left lateral view. As in the Zambian specimen, the lateral dentary shelf closely approaches the dorsal edge of the dentary (2) in lateral view. **D**, Detail of a partially erupted left dentary tooth exposed in lingual view along a natural break in NMT RB1136. The tooth bears prominent distal denticles (3). **E**, Partial dentary of *C. helmoedi* from Tanzania (NMT RB1254) in left lateral view. As in the Zambian specimen, the lateral dentary shelf closely approaches the dorsal edge of the dentary (4) in lateral view. **F**, Zambian mandible of *C. helmoedi* (NHCC LB211) in dorsal view for comparison. **G**, Partial dentary of *C. helmoedi* from Tanzania (NMT RB1100) in dorsal view. As in the Zambian specimen, the posterior dentary sulcus has a medial expansion at its anterior end (5) and a transverse ridge is present on the dorsal surface of the lateral dentary shelf (6). **H**, Partial dentary of *C. helmoedi* from Tanzania (NMT RB1136) in dorsal view. As in the Zambian specimen, the posterior dentary sulcus has a medial expansion at its anterior end (7). **I**, Partial dentary of *C. helmoedi* from Tanzania (NMT RB1254) in dorsal view. As in the Zambian specimen, the posterior dentary sulcus has a medial expansion at its anterior end (8) and a transverse ridge is present on the dorsal surface of the lateral dentary shelf (9). **J**, Partial dentary from Tanzania (NHMUK PV R 12453) described by Angielczyk & Cox (2015) in left lateral view (photo by P. Hurst). The specimen differs from *C. helmoedi* by having a lateral dentary shelf that does not closely approach the dorsal edge of the dentary in lateral view (10). **K**, Partial dentary from Tanzania (NMT RB230) described by Angielczyk & Cox (2015) in right lateral view. The specimen differs from *C. helmoedi* by having a lateral dentary shelf that does not closely approach the dorsal edge of the dentary in lateral view (11) and an elongate groove on the lateral surface of the lateral dentary shelf (12). **L**, Partial dentary from Tanzania (NHMUK PV R 12453) described by Angielczyk & Cox (2015) in dorsal view. The specimen differs from *C. helmoedi* by having fewer dentary teeth (13) and lacking a posterior dentary sulcus (14). **M**, Partial dentary from Tanzania (NMT RB230) described by Angielczyk & Cox (2015) in dorsal view. The specimen differs from *C. helmoedi* by having fewer dentary teeth (15) and lacking a posterior dentary sulcus (16). Scale bars are 2 cm. The upper scale bar applies to panels A–I; the lower scale bar applies to panels J–M.

shelf is preserved. The shelf is large, and its anterior portion angles anteromedially (Fig. 4G), giving it a triangular shape in dorsal view similar to that of NHCC LB211. A weak transverse ridge is present on the dorsal surface near the widest point of the shelf (Fig. 4G), although it is less prominent than in NHCC LB211. In lateral view, the lateral dentary shelf approaches the dorsal margin of the dentary (Fig. 4B). A series of low ridges is present on the lateral surface of the shelf, likely representing a muscle scar, but they do not form a prominent, raised attachment area such as that seen in *Emydops*. The posterior part of the lateral dentary shelf is not preserved, so it is uncertain whether the oval fossa observed on the lateral surface in that area of NHCC LB211 was present in NMT RB1100.

NMT RB1136 is the most fragmentary of the three specimens and consists of the anterior portion of the left dentary ramus (Fig. 4C,D,H). As preserved, there appears to be a total of six tooth positions in the dentary. The first and third positions are occupied by broken teeth, and a tooth with a well-preserved crown is in the process of erupting in the second position. Positions four through six are represented by empty alveoli. The crown in the second position is blade-like and laterally compressed, with coarse distal denticles (Fig. 4D), similar to the dentary teeth of NHCC LB211. The symphyseal portion of the ramus is damaged, but enough is preserved to show that the dentary table was absent (Fig. 4H). The posterior dentary sulcus is present, and it has a rounded medial expansion at its anterior end that is comparable to that in NHCC LB211 (Fig. 4F,H). Only a small anterior portion of the lateral dentary shelf is preserved, but this approaches the dorsal margin of the dentary and its anterior portion angles anteromedially (Fig. 4C).

NMT RB1254 includes a complete dentary symphysis and the anterior portions of the left and right dentary rami Fig. 4E,I). At least four tooth positions are present in the left dentary, the first of which preserves a partially erupted crown that is laterally compressed and blade-like, with coarse distal denticles. The second and third positions house the roots of highly damaged teeth, and posterior to this are the remains of a displaced, fourth tooth. The right side preserves four to five tooth positions. The first two are occupied by the roots of incomplete teeth. The remaining positions consist of empty alveoli, and damage makes the identification of the putative fifth position tentative. Both sides of the jaw clearly show that the dentary table was absent (Fig. 4I); instead, the dorsal surface of the dentary immediately posterior to the symphysis has the form of a rounded ridge. The posterior dentary sulcus is present, and it has a rounded medial expansion at its anterior end (best seen on the right side) (Fig. 4I). Little of the lateral dentary shelf is present on either side of the jaw. However, enough is preserved to show that its anterior portion angled anteromedially and that it closely approached the dorsal margin of the dentary (Fig. 4E). The damaged remains of a transverse ridge on the dorsal surface of the shelf are preserved on the right side of the specimen (Fig. 4I).

Although all three of these specimens are fragmentary, they all present a combination of characters that supports referral to *C. helmoedi*. Specifically, the specimens lack a dentary table, and they possess dentary teeth, a posterior dentary sulcus with a rounded medial expansion at its anterior end, and a lateral dentary shelf that closely approaches the dorsal margin of the dentary. Furthermore, based on the comparisons above, this combination of characters allows us to reject *Pristerodon* and *Emydops* as potential identifications for the specimens.

THE IDENTITY OF NHMUK PV R 12453 AND NMT RB230

Angielczyk & Cox (2015) described two small, toothed dicynodont jaws from the Ruhuhu Basin of Tanzania. One of the specimens (NHMUK PV R 12453; Fig. 4J,L) originated in the Ruhuhu Formation, and the other (NMT RB230; Fig. 4K,M) was collected in the Usili Formation, and the authors suggested the specimens likely represent a single, stratigraphically long-ranging taxon. At the time of writing of that paper, the mandible of *C. helmoedi* was unknown, and Angielczyk & Cox (2015) considered the possibility the specimens might represent *C. helmoedi*, among other possible identifications. The new anatomical information provided by the mandible of NHCC LB211 and the three new Tanzanian specimens refutes this hypothesis. Both NHMUK PV R 12453 and NMT RB230 lack a posterior dentary sulcus (Fig. 4L,M), and the tooth rows of the specimens are shorter than those observed in NHCC LB211 and the new Tanzanian specimens (1–2 erupted teeth with potential space for a third tooth *versus* 4–7 tooth positions). The lateral dentary shelf is prominent in NHMUK PV R 12453 and NMT RB230 but the shelf does not closely approach the dorsal margin of the dentary (Fig. 4J,K), and the more complete shelf in NMT RB230 has a more sigmoidal profile in lateral view (Fig. 4K) than is the case for NHCC LB211. A fossa is present on the dorsal surface of the lateral dentary shelf, and although its lateral and anterior margins are somewhat thickened (best seen on the right side of NHMUK PV R 12453) a strong transverse ridge comparable to that in NHCC LB211 is absent (Fig. 4J,K). Angielczyk & Cox (2015) reported a fossa on the lateral surface of the lateral dentary shelf in NMT RB230, but it has the form of a very shallow elongate channel in that specimen (Fig. 4K), as opposed to the more discrete oval fossa present in NHCC LB211. Finally, in NMT RB230 a thin lamina of bone extends a considerable distance ventrally from the the bottom of the lateral dentary shelf (Fig. 4K). The ventral and posterior edges of the lamina are incomplete, but this morphology is highly suggestive of the external mandibular fenestra being occluded laterally by a lamina of the dentary, similar to the condition in *Dicynodontoides*, *Kombuisia*, and possibly *Thliptosaurus* (Cox 1959; Fröbisch 2007; Angielczyk & Cox 2015; Kammerer 2019; Macungo *et al*. 2022). By contrast, the mandibular fenestra is open laterally in NHCC LB211 and opens directly below the lateral dentary shelf. Although the new specimens demonstrate that NHMUK PV R 12453 and NMT RB230 are not additional Tanzanian records of *C. helmoedi*, they do not completely resolve the question of their identity. Additional discoveries will be required to determine whether

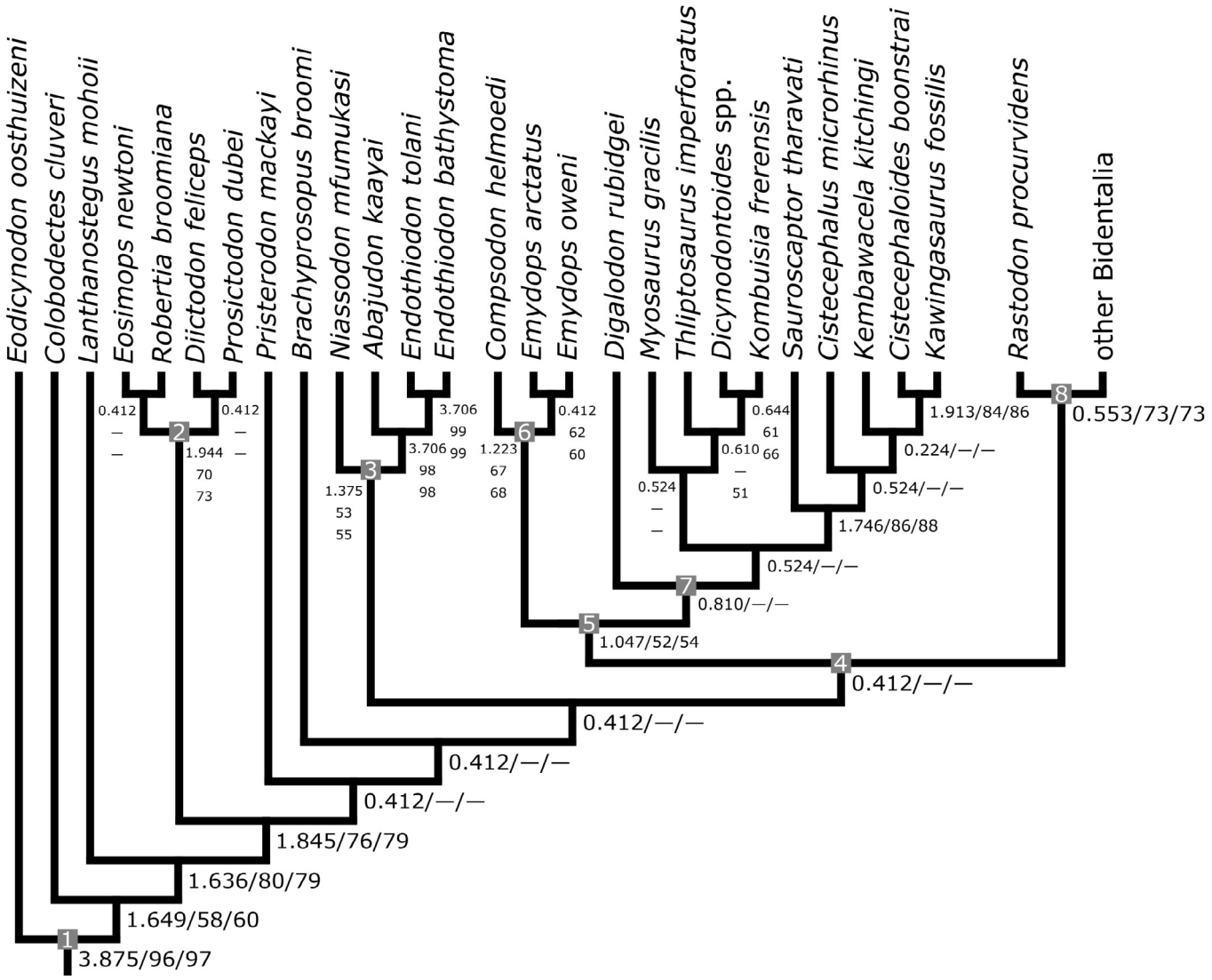

Figure 5. Detail of the strict consensus of the five most parsimonious cladograms (length 1224.917; consistency index = 0.226; retention index = 0.717). Numbers at nodes represent decay index (left/top), symmetric resampling (middle), and jackknife (bottom/right) values. Symmetric resampling and jackknife scores of less than 50% are not shown. Numbered nodes: 1, Dicynodontia; 2, Pylaecephalidae; 3, Endothiodontia; 4, Therochelonia; 5, Emydopoidea; 6, Emydopidae; 7, Kistecephalia; 8, Bidentalia.

NHMUK PV R 12453 and NMT RB230 represent a new taxon, a rare variant of *Dicynodontoides*, or the 'missing' mandible of another previously known taxon such as *Cryptocynodon* (see Angielczyk & Cox [2015] for further discussion).

PHYLOGENETIC RESULTS AND IMPLICATIONS

Five most parsimonious cladograms of length 1224.917 (consistency index = 0.226, retention index = 0.717) were recovered by the new technology search; no additional cladograms were found by the traditional search. The portion of the strict consensus tree covering non-bidentalian dicynodonts is presented in Fig. 5. The topology of this portion of the tree is essentially identical to that presented in Angielczyk *et al*. (2021), including recovering the two species of *Emydops* and *Compsodon* as members of a monophyletic Emydopidae, but it differs from that of Angielczyk *et al*. (2019) in the earlier-diverging position of Emydopidae. It also differs more substantially from the results of Macungo *et al*. (2022), presumably on account of the fact that the braincase characters they added to their dataset were not included in the version of the dataset used here. Notably, the analysis also recovered *Rastodon* as a basal bidentalian instead of a member of Emydopoidea, a possibility discussed by Kammerer & Ordoñez (2021) and Macungo *et al*. (2022). Compared to the Angielczyk *et al*. (2021) results, the addition of mandible codings for *C. helmoedi* slightly altered symmetric resampling and jackknife support for Emydopidae and the values for some of the surrounding nodes, but the differences are small enough to essentially be insignificant. The Bremer support value for Emydopidae did not change, but the new codings caused a slight increase in the support values for several of the surrounding nodes (e.g. Endothiodontia, Kistecephalia). Four discrete-state synapomorphies diagnose Emydopidae in the analysis: posterior median ridge on palatal surface of premaxilla present with a flattened, expanded anterior area (character 5, state 1); maxillary non-caniniform teeth located near lateral margin of maxilla (ch. 23, st. 0); ventral edge of the caniniform process or dorsal edge of the erupted portion of the canine tusk at the same level to slightly posterior to

the anterior orbital margin (ch. 32, st. 1); and lateral edge of paroccipital process drawn into sharp posteriorly-directed process that is distinctly offset from the surface of the occipital plate present (ch. 112, st. 1). None of the newly coded mandibular characters serve as synapomorphies for Emydopidae, but several of the characters related to the dentary teeth (which are lost in kistecephalians) are reconstructed as emydopid symplesiomorphies that differentiate the clade from kistecephalians.

A recent issue in studies of dicynodont phylogeny concerns relationships at the base of Therochelonia, including the questions of whether pylaecephalids and endothiodonts fall within Therochelonia (as part of the emydopoid lineage), as well as whether the Brazilian dicynodont *Rastodon procurvidens* may be a kingoriid emydopoid instead of an early bidentalian as is commonly assumed (Angielczyk & Kammerer 2017; Olroyd *et al*. 2018; Angielczyk *et al*. 2019; Kammerer & Ordoñez 2021; Macungo *et al*. 2022). Because the new character data for *C. helmoedi* provides additional information about character states near the base of Emydopoidea and Therochelonia, our phylogenetic results have some bearing on this discussion.

In our most parsimonious cladograms, Pylaecephalidae falls in a relatively stemward position among dicynodonts, and endothiodonts are reconstructed as the sister-group of Therochelonia. Only three discrete-state synapomorphies support the monophyly of Therochelonia exclusive of Endothiodontia: maxillary non-caniniform teeth absent (ch. 23, st. 2); mid-ventral plate of vomers without a notable expanded area posterior to junction with premaxilla (ch. 72, st. 1); and mid-ventral plate of vomers narrow and blade-like in ventral view (ch. 73, st. 1). However, in each case the therochelonian state is near ubiquitous within the clade, and very rare or never observed in earlier-diverging taxa aside from the pylaecephalid *Diictodon*. Interestingly, the parsimony optimization of character 23 implies that the presence of maxillary 'postcanines' in Emydopidae is a reversal from a toothless ancestor, but this stems from the fact that the more laterally placed teeth in emydopids received a different coding than the more medial teeth found in endothiodonts, pylaecephalids, *Pristerodon*, and *Brachyprosopus*. Recoding the character as binary (i.e. simply the presence or absence of maxillary 'postcanines') results in an ambiguous optimization at the base of Therochelonia, Emydopoidea, and Bidentalia, because it is not known whether maxillary 'postcanines' were present in *Rastodon* (Boos *et al*. 2016; Simão-Oliveira *et al*. 2020). However, one of the equally parsimonious optimizations in that scenario is that maxillary 'postcanines' were present in the common ancestor of Emydopoidea, which seems plausible given the relatively early first appearance of the toothed taxon *Emydops* in the fossil record (e.g. Angielczyk *et al*. 2005; Day *et al*. 2018; Day & Rubidge 2020) and the basal position of Emydopidae within Emydopoidea. If the more nested position of Emydopidae within Emydopoidea proposed by Macungo *et al*. (2022) is correct, it would provide additional support for the reversal hypothesis because several toothless taxa (*Dicynodontoides*, *Kombuisia*, *Thliptosaurus*, *Digalodon*) would fall at the base of the clade before the divergence of the toothed emydopids.

Four discrete-state synapomorphies diagnose Bidentalia (including *Rastodon*) in our analysis: snout open to back of the skull (ch. 16, st. 0); keel-like extension of the palatal rim posterior to the caniniform process absent (ch. 30, st. 0); parietals exposed in midline groove or channel (ch. 49, st. 1); and prootic bearing rectangular alar process that forms a plate raised above surface of temporal fenestra wall, in front of fossa absent (ch. 108, st. 0). All of these character states are present in *Rastodon*, but are rare or absent among emydopoids. Therefore, there is relatively firm character support for the placement of *Rastodon* within Bidentalia, despite the similarities to kingoriid emydopoids noted by Kammerer & Ordoñez (2021) and Macungo *et al*. (2022) (e.g. elongate dentary symphysis, partial occlusion of mandibular fenestra by a lamina of the dentary; notch in the palatal rim anterior to the caniniform process). Kammerer & Ordoñez (2021) underscored the need for additional character data to further test the phylogenetic position of *Rastodon*, and to the examples they mentioned we add the need for information on whether 'postcanine' teeth are present in the maxilla and dentary of the taxon. *Rastodon* is currently coded as uncertain for these characters (and related characters that describe the morphology of the teeth) because the mandible is preserved in occlusion with the palate in the only known specimen, and this complicates the optimization of these characters at the base of Therochelonia, Emydopoidea, and Bidentalia. It should be possible to assess whether 'postcanines' are present in *Rastodon* using the CT data that exist for the taxon (Simão-Oliveira *et al*. 2020), and if they are present, it would be very interesting to know whether that, along with the other characters noted by Kammerer & Ordoñez (2021), would be enough to move it into Emydopoidea.

BIOSTRATIGRAPHIC IMPLICATIONS

Since their discovery in the first half of the 20th century, there has been general agreement that the tetrapod assemblages of the Upper Madumabisa Mudstone Formation in the Luangwa Basin and the Usili Formation of the Ruhuhu Basin can be correlated with the late Permian-aged assemblages of the Karoo Basin (e.g. Haughton 1932; Boonstra 1938; von Huene 1950; Drysdall & Kitching 1963; Kemp 1975; Wild *et al*. 1993; King & Jenkins 1997; Lucas 1998, 2006; Gay & Cruickshank 1999; Rubidge 2005), potentially encompassing parts or all of the modern *Endothiodon*, *Cistecephalus*, and *Daptocephalus* assemblage zones of the Karoo (Day & Smith 2020; Smith 2020; Viglietti 2020). However, problems such as taxonomic confusion, uncertainty as to the exact geographic and stratigraphic positions of historical localities, and the absence of radiometric dates made precise correlations difficult. As our research group began work in the Luangwa and Ruhuhu basins, our initial data suggested that a correlation between the Upper Madumabisa Mudstone assemblage, the Usili Formation assemblage, and the *Cistecephalus* Assemblage Zone of South Africa likely was the best-supported possibility, although some discrepancies

persisted between basins in the apparent stratigraphic ranges of taxa (e.g. Sidor *et al*. 2010; Angielczyk *et al*. 2014a,b; also see Angielczyk 2002). Further research has not resolved this problem. Instead, evidence is accumulating that the Upper Madumabisa Mudstone assemblage in particular may span the temporal boundary between the *Cistecephalus* and *Daptocephalus* assemblage zones and/or hosts two distinct faunal assemblages (Huttenlocker & Abdala 2015; Angielczyk & Kammerer 2017; Angielczyk 2019; Huttenlocker & Sidor 2020; Peecook *et al*. 2020; Kammerer *et al*. 2022). An additional complication is the recent discovery that the Karoo *Cistecephalus* Assemblage Zone itself is problematic, with low-resolution occurrence data for many specimens leading to poorer statistical support for the assemblage zone than for the overlying *Daptocephalus* and *Lystrosaurus declivis* assemblage zones (Viglietti *et al*. 2022). The South African specimens of *Compsodon* are intimately entangled in this issue because one of the historical specimens with relatively low resolution locality information was collected on the farm Boskraal in Oudeberg Pass near Graaff-Reinet, which hosts exposures of the upper *Cistecephalus* Assemblage Zone and the lower *Daptocephalus* Assemblage Zone (Angielczyk & Kammerer 2017).

The discovery of the new *Compsodon* specimens described here may contribute to the eventual development of more refined biostratigraphic correlations between the Karoo, Luangwa, and Ruhuhu basins, but they are insufficient to solve the problem on their own. Like the Zambian *Compsodon* specimens described by Angielczyk & Kammerer (2017), NHCC LB211 was collected relatively high in the Upper Madumabisa Mudstone Formation, making it part of the upper faunal assemblage proposed by Peecook *et al*. (2020) and the subject of research in progress. The three new Tanzanian *Compsodon* mandibles were collected in the upper half of the Usili Formation, in strata falling in the Middle Grey Mudrock and the Upper Pebbly Sandstone of Kaaya (1992) and Angielczyk *et al*. (2014a). At the broadest scale, the relatively high stratigraphic occurrences of the Tanzanian and Zambian specimens potentially favour an additional biostratigraphic link between the Upper Madumabisa Mudstone Formation, the Usili Formation, and the *Daptocephalus* Assemblage Zone (*sensu* Viglietti 2020) instead of the underlying *Cistecephalus* Assemblage Zone. However, this observation provides a very limited advance in our biostratigraphic knowledge until it is possible to say with more certainty whether *Compsodon* also occurs in the *Cistecephalus* zone in South Africa.

The fact that the three Tanzanian mandibles fall within the upper half of the Usili Formation raises the possibility of subdividing its faunal assemblage in a manner analogous to that proposed for the Upper Madumabisa Mudstone Formation. Further research on tetrapod occurrences in the Usili Formation will be needed before such a subdivision can be justified, though, particularly considering that some taxa appear to have stratigraphic ranges that span most of the Usili Formation and extend into the underlying Ruhuhu Formation (Angielczyk *et al*. 2014a; Angielczyk & Cox 2015). Additional specimens of *Compsodon* from South Africa also are needed to better delineate its stratigraphic range in the Karoo Basin, especially if the *Cistecephalus* Assemblage Zone requires new scrutiny as a weakly supported biostratigraphic unit. Nevertheless, the new Tanzanian record of *Compsodon* corroborates previous suggestions that small dicynodonts were effective dispersers in southern and eastern Africa during the Permian (Angielczyk & Sullivan 2008; Angielczyk & Kammerer 2017; Angielczyk 2019), and that they may have biostratigraphic utility if their stratigraphic and temporal ranges can be sufficiently well constrained.

ABBREVIATIONS

Institutional

BP	Evolutionary Studies Institute, Johannesburg, South Africa
NHCC	National Heritage Conservation Commission, Lusaka, Zambia
NHMUK	Natural History Museum, London, United Kingdom
NMT	National Museum of Tanzania, Dar es Salaam, Tanzania
RC	Rubidge Collection, Graaff-Reinet, South Africa
SAM	Iziko South African Museum, Cape Town, South Africa

We are very pleased to dedicate this paper to our friend, colleague, and collaborator Bruce Rubidge. For more than three decades, Bruce has stood at the forefront of South African palaeontology, both in terms of the number and scope of his scientific contributions and his tireless efforts to help the field as a whole realize its immense scientific potential. Like so many Karoo workers, we have benefited greatly from Bruce's wisdom, advice, assistance, and generosity, and we're thrilled to have the opportunity to say, 'Thank you, Bruce!' We also thank our many friends who have assisted with fieldwork in Tanzania and Zambia, particularly the members of the 2009 Zambia team (A. Goulding, K. Mwamulowe, J. Menke, C. Sidor, J-S. Steyer, S. Tolan, R. Whatley) and the 2017 Tanzania team (J. Fortner, J. Lungmus, S. Nesbitt, S. Olroyd, C. Sidor, J-S. Steyer, M. Stocker, A. Tibaijuka). A. Tibaijuka and K. Mwamulowe deserve special thanks for their assistance in obtaining research and export permits in Tanzania and Zambia, respectively. Funding for fieldwork was provided by the National Geographic Society (CRE 8571-08 to J-S. Steyer; CRE 9606-14 to S. Nesbitt; NGS 158R-18 to B.R.P.), the National Science Foundation (EAR-1337281 to K.D.A. and S. Nesbitt; EAR-1337569 to C. Sidor), and The Field Museum/IDP Foundation, Inc. African Training and African Partner programs (to K.D.A.). J. Aramini and A. Shinya prepared the specimens, and A. Neander and J. Lungmus provided assistance with CT-scanning. J. Fröbisch, C. Sullivan, and an anonymous reviewer provided helpful suggestions that improved the manuscript, and handling editor C. Kammerer provided important historical information that allowed us to correct the taxonomic authority for Dicynodontia.

§ORCID iDs

K.D. Angielczyk: orcid.org/0000-0001-7147-2054
B.R. Peecook: orcid.org/0000-0002-0566-1487
R.M.H. Smith: orcid.org/0000-0001-6806-1983

REFERENCES

ANGIELCZYK, K.D. 2001. Preliminary phylogenetic analysis and stratigraphic congruence of the dicynodont anomodonts (Synapsida: Therapsida). *Palaeontologia africana* **37**, 53–79.

ANGIELCZYK, K.D. 2002. Redescription, phylogenetic position, and stratigraphic significance of the dicynodont genus *Odontocyclops* (Synapsida: Anomodontia). *Journal of Paleontology* **76**, 1047–1059.

ANGIELCZYK, K.D. 2019. First occurrence of the dicynodont *Digalodon* (Therapsida, Anomodontia) from the Lopingian Upper Madumabisa Mudstone Formation, Luangwa Basin, Zambia. *Palaeontologia africana* **53**, 219–225.

ANGIELCZYK, K.D. & COX, C.B. 2015. Distinctive emydopoid dicynodont (Therapsida, Anomodontia) mandibles from the Permian Ruhuhu and Usili Formations (Songea Group), Ruhuhu Basin, Tanzania. *Journal of Vertebrate Paleontology*. DOI: 10.1080/02724634.2015.1008699

ANGIELCZYK, K.D. & KAMMERER, C.F. 2017. The cranial morphology, phylogenetic position, and biogeography of the Upper Permian dicynodont *Compsodon helmoedi* van Hoepen (Therapsida, Anomodontia). *Papers in Palaeontology* **3**, 513–545.

ANGIELCZYK, K.D. & RUBIDGE, B.S. 2013. Skeletal morphology, phylogenetic relationships and stratigraphic range of *Eosimops*

newtoni Broom, 1921, a pylaecephalid dicynodont (Therapsida, Anomodontia) from the Middle Permian of South Africa. *Journal of Systematic Palaeontology* **11**, 191–231.
ANGIELCZYK, K.D. & SULLIVAN, C. 2008. *Diictodon feliceps* (Owen, 1876), a dicynodont (Therapsida, Anomodontia) species with a Pangaean distribution. *Journal of Vertebrate Paleontology* **28**, 788–802.
ANGIELCZYK, K.D., BENOIT, J. & RUBIDGE, B.S. 2019. A new tusked cistecephalid dicynodont (Therapsida, Anomodontia) from the upper Permian Upper Madumabisa Mudstone Formation, Luangwa Basin, Zambia. *Papers in Palaeontology* **7**, 405–446.
ANGIELCZYK, K.D., FRÖBISCH, J. & SMITH, R.M.H. 2005. On the stratigraphic range of the dicynodont taxon *Emydops* (Therapsida: Anomodontia) in the Karoo Basin, South Africa. *Palaeontologia africana* **41**, 23–33.
ANGIELCZYK, K.D., LIU, J. & YANG, W. 2021. A redescription of *Kunpania scopulusa*, a bidentalian dicynodont (Therapsida, Anomodontia) from the ?Guadalupian of northwestern China. *Journal of Vertebrate Paleontology*.
DOI: 10.1080/02724634.2021.1922428
ANGIELCZYK, K.D., RUBIDGE, B.S., DAY, M.O. & LIN, F. 2016. A reevaluation of *Brachyprosopus broomi* and *Chelydontops altidentalis*, dicynodonts (Therapsida, Anomodontia) from the Middle Permian *Tapinocephalus* Assemblage Zone of the Karoo Basin, South Africa. *Journal of Vertebrate Paleontology* **36**, e1078342.
ANGIELCZYK, K.D., HUERTAS, S., SMITH, R.M.H., TABOR, N.J., SIDOR, C.A., STEYER, J-S., TSUJI, L A. & GOSTLING, N.J. 2014a. New dicynodonts (Therapsida, Anomodontia) and updated tetrapod stratigraphy of the Permian Ruhuhu Formation (Songea Group, Ruhuhu Basin) of southern Tanzania. *Journal of Vertebrate Paleontology* **34**, 1408–1426.
ANGIELCZYK, K.D., STEYER, J.S., SIDOR, C.A, SMITH, R.M.H., WHATLEY, R.L. & TOLAN, S. 2014b. Permian and Triassic dicynodont (Therapsida: Anomodontia) faunas of the Luangwa Basin, Zambia: taxonomic update and implications for dicynodont biogeography and biostratigraphy. **In**: Kammerer, C.F., Angielczyk, K.D. & Fröbisch (eds), *Early Evolutionary History of the Synapsida*, 93–138. Dordrecht, Springer.
BOONSTRA, L.D. 1938. A report on some Karroo reptiles from the Luangwa Valley, Northern Rhodesia. *Quarterly Journal of the Geological Society of London* **94**, 371–384.
BOOS, A.D.S., KAMMERER, C.F., SCHULTZ, C.L., SOARES, M.B. & ILHA, A.L.R. 2016. A new dicynodont (Therapsida: Anomodontia) from the Permian of southern Brazil and its implications for bidentalian origins. *PLOS ONE* **11**(5), e0155000.
BREMER, K. 1988. The limits of amino acid sequence data in angiosperm phylogenetic reconstruction. *Evolution* **42**, 795–803.
BREMER, K. 1994. Branch support and tree stability. *Cladistics* **10**, 295–304.
BROOM, R. 1905. On the use of the term Anomodontia. *Records of the Albany Museum* **1**, 266–269.
CLUVER, M.A. 1974. The skull and mandible of a new cistecephalid dicynodont. *Annals of the South African Museum* **66**, 137–155.
COX, C.B. 1959. On the anatomy of a new dicynodont genus with evidence of the position of the tympanum. *Proceedings of the Zoological Society of London* **132**, 321–367.
COX, C.B. 1964. On the palate, dentition, and classification of the fossil reptile *Endothiodon* and related genera. *American Museum Novitates* **2171**, 1–25.
CROMPTON, A.W. & HOTTON, N. III 1967. Functional morphology of the masticatory apparatus of two dicynodonts (Reptilia, Therapsida). *Postilla* **109**, 1–51.
DAY, M.O. & RUBIDGE, B.S. 2020. Biostratigraphy of the *Tapinocephalus* Assemblage Zone (Beaufort Group, Karoo Supergroup), South Africa. *South African Journal of Geology* **123**, 149–164.
DAY, M.O. & SMITH, R.M.H. 2020. Biostratigraphy of the *Endothiodon* Assemblage Zone (Beaufort Group, Karoo Supergroup), South Africa. *South African Journal of Geology* **123**, 165–180.
DAY, M.O., BENSON, R.B.J., KAMMERER, C.F. & RUBIDGE, B.S. 2018. Evolutionary rates of mid-Permian tetrapods from South Africa and the roles of temporal resolution in turnover reconstruction. *Paleobiology* **44**, 347–367.
DRYSDALL, A.R. & KITCHING, J.W. 1963. A re-examination of the Karroo succession and fossil localities of part of the upper Luangwa Valley. *Geological Survey of Northern Rhodesia Memoir* **1**, 1–62.
FARRIS, J.S., ALBERT, V.A, KÄLLERSJÖ, M., LIPSCOMB, D. & KLUGE, A.G. 1996. Parsimony jackknifing outperforms neighbor-joining. *Cladistics* **12**, 99–124.
FRÖBISCH, J. 2007. The cranial anatomy of *Kombuisia frerensis* Hotton (Synapsida, Dicynodontia) and a new phylogeny of anomodont therapsids. *Zoological Journal of the Linnean Society* **150**, 117–144.
FRÖBISCH, J. & REISZ, R.R. 2008. A new species of *Emydops* (Synapsida, Anomodontia) and a discussion of dental variability and pathology in dicynodonts. *Journal of Vertebrate Paleontology* **28**, 770–787.
FRÖBISCH, J., ANGIELCZYK, K.D. & SIDOR, C.A. 2010. The Triassic dicynodont *Kombuisia* (Synapsida, Anomodontia) from Antarctica, a refuge from the terrestrial Permian-Triassic mass extinction. *Naturwissenschaften* **97**, 187–196.
GAY, S.A. & CRUICKSHANK, A.R.I. 1999. Biostratigraphy of the Permian tetrapod faunas from the Ruhuhu Valley, Tanzania. *Journal of African Earth Sciences* **29**, 195–210.
GOLOBOFF, P.A. & CATALANO, S.A. 2016. TNT version 1.5, including a full implementation of phylogenetic morphometrics. *Cladistics* **32**, 221–238.
GOLOBOFF, P.A. & MORALES, M.E. 2023. TNT version 1.6, with a graphical interface for MacOS and Linux, including new routines in parallel. *Cladistics* **39**, 144– 153
GOLOBOFF, P.A., FARRIS, J.S. & NIXON, K.C. 2008. TNT, a free program for phylogenetic analysis. *Cladistics* **24**, 774–786.
GOLOBOFF, P.A., MATTONI, C.I. & QUINTEROS, A.S. 2006. Continuous characters analyzed as such. *Cladistics* **22**, 589–601.
GOLOBOFF, P.A., FARRIS, J.S., KÄLLERSJÖ, M., OXELMAN, B., RAMÍREZ, M.J. & SZUMIK, C.A. 2003. Improvements to resampling measures of group support. *Cladistics* **19**, 324–332.
HAUGHTON, S.H. 1932. On a collection of Karroo vertebrates from Tanganyika Territory. *Quarterly Journal of the Geological Society of London* **88**, 634–671.
HUENE, F. VON. 1950. Die Theriodontier des ostafrikanischen Ruhuhu-Gebietes in der Tübinger Sammlung. *Neues Jahrbuch für Geologie und Paläontologie, Abhandlungen* **92**, 47–136.
HUTTENLOCKER, A.K. & ABDALA, F. 2015. Revision of the first therocephalian, *Theriognathus* Owen (Therapsida: Whaitsiidae), and implications for cranial ontogeny and allometry in nonmammaliaform eutheriodonts. *Journal of Paleontology* **89**, 645–664.
HUTTENLOCKER, A.K. & SIDOR, C.A. 2020. A basal nonmammaliaform cynodont from the Permian of Zambia and the origins of mammalian endocranial and postcranial anatomy. *Journal of Vertebrate Paleontology*.
DOI: 10.1080/02724634.2020.1827413
KAAYA, C.Z. 1992. Depositional environment of Late Permian Karoo beds in the Ruhuhu Basin and Mikumi area of Tanzania. *Geologisches Institut der Universität zu Köln Sonderveröffentlichungen* **83**, 1–126.
KAMMERER, C.F. 2019. A new dicynodont (Anomodontia: Emydopoidea) from the terminal Permian of KwaZulu-Natal, South Africa. *Palaeontologia africana* **53**, 197–191.
KAMMERER, C.F. & ORDOÑEZ M. DE LOS A. 2021. Dicynodonts (Therapsida: Anomodontia) of South America. *Journal of South American Earth Sciences* **108**, 103171.
KAMMERER, C.F., ANGIELCZYK, K.D. & FRÖBISCH, J. 2011. A comprehensive taxonomic revision of *Dicynodon* (Therapsida, Anomodontia) and its implications for dicynodont phylogeny, biogeography, and biostratigraphy. *Society of Vertebrate Paleontology Memoir* **11**, 1–158.
KAMMERER, C.F., ANGIELCZYK, K.D. & FRÖBISCH, J. 2015a. Redescription of *Digalodon rubidgei*, an emydopoid dicynodont (Therapsida, Anomodontia) from the Late Permian of South Africa. *Fossil Record* **18**, 43–55.
KAMMERER, C.F., ANGIELCZYK, K.D. & FRÖBISCH, J. 2015b. Redescription of the geikiid *Pelanomodon* (Therapsida, Dicynodontia), with a reconsideration of '*Propelanomodon*.' *Journal of Vertebrate Paleontology*.
DOI: 10.1080/02724634.2015.1030408
KAMMERER, C.F., ARAÚJO, R., CUMBANE, K., MACUNGO, Z. SMITH, R.M.H. & ANGIELCZYK, K.D. 2022. New material of *Dicynodon angielczyki* (Synapsida: Anomodontia) from Mozambique and Zambia with biostratigraphic implications for Permo-Triassic basins. *Journal of Vertebrate Paleontology*.
DOI: 10.1080/02724634.2021.2041652
KEMP, T.S. 1975. Vertebrate localities in the Karroo System of the Luangwa Valley, Zambia. *Nature* **254**, 415–416.
KING, G.M. & JENKINS, I. 1997. The dicynodont *Lystrosaurus* from the Upper Permian of Zambia: evolutionary and stratigraphical implications. *Palaeontology* **40**, 149–156.
KOPUCHIAN, C. & RAMÍREZ, M.J. 2010. Behaviour of resampling methods under different weighting schemes, measures and variable sampling strengths. *Cladistics* **26**, 86–97.
LIU, J. 2020. *Taoheodon baizhijuni*, gen. et sp. nov. (Anomodontia, Dicynodontoidea), from the upper Permian Sunjiagou Formation of China and its implications. *Journal of Vertebrate Paleontology*.
DOI: 10.1080/02724634.2020.1762088
LUCAS, S.G. 1998. Toward a tetrapod biochronology of the Permian. *New Mexico Museum of Natural History and Science Bulletin* **12**, 71–91.

LUCAS, S.G. 2006. Global Permian tetrapod biostratigraphy and biochronology. **In**: Lucas, S.G., Cassinis, G. & Schneider, J.W. (eds), Non-marine Permian biostratigraphy and biochronology. *Geological Society of London Special Publications* **265**, 65–93.

MACUNGO, Z., LOIDE, I., ZUNGUZA, S., NHAMUTOLE, N., MAHARAJ, I.E.M., MUGABE, J., ANGIELCZYK, K.D. & ARAÚJO, R. 2020. *Endothiodon* (Therapsida, Anomodontia) specimens from the middle/late Permian of the Metangula Graben (Niassa Province, Mozambique) increase complexity to the taxonomy of the genus. *Journal of African Earth Sciences* **185**, 103647.

MACUNGO, Z., BENOIT, J., FERNANDEZ, V & ARAÚJO, R.M.N. 2022. X-ray microcomputed and synchrotron tomographic analysis of the basicranial axis of emydopoid dicynodonts: implications for fossoriality and phylogeny. *Zoological Journal of the Linnean Society* **198**, 1–46.

MUELLER, L.D. & AYALA, F.J. 1982. Estimation and interpretation of genetic distance in empirical studies. *Genetical Research* **40**, 127–137.

OLIVIER, C., BATTAIL, B., BOURQUIN, S. ROSSIGNOL, C., STEYER, J-S. & JALIL, N.E. 2019. New dicynodonts (Therapsida, Anomodontia) from near the Permo-Triassic boundary of Laos: implications for dicynodont survivorship across the Permo-Triassic mass extinction and the paleobiogeography of Southeast Asian blocks. *Journal of Vertebrate Paleontology*.
DOI: 10.1080/02724634.2019.1584745

OLROYD, S.L., SIDOR, C.A. & ANGIELCZYK, K.D. 2018. New materials of the enigmatic dicynodont *Abajudon kaayai* (Therapsida, Anomodontia) from the lower Madumabisa Mudstone Formation, middle Permian of Zambia. *Journal of Vertebrate Paleontology*.
DOI: 10.1080/02724634.2017.1403442

OLROYD, S.L., LEBLANC, A.R.H., ARAÚJO, R., ANGIELCZYK, K.D., DUHAMEL, A., BENOIT, J. & AMARAL, M. 2021. Histology and μCT reveal the unique evolution and development of multiple tooth rows in the synapsid *Endothiodon*. *Scientific Reports* **11**, 16875.

OWEN, R. 1859. On some reptilian remains from South Africa. *Edinburgh New Philosophical Journal* **10**, 289–291.

OWEN, R. 1860. On the orders of fossil and Recent Reptilia, and their distribution in time. *Report of the 29th Meeting of the British Association for the Advancement of Science (1859)*, 153–166.

PEECOOK, B.R., ANGIELCZYK, K.D., KAMMERER, C.F., LUNGMUS, J.K., McINTOSH, J.A., SIDOR, C.A., SMITH, R.M.H., TOLAN, S., VIGLIETTI, P.A. & WHITNEY, M.R. 2020. A new stratigraphic framework for the Permo-Triassic strata of the Luangwa Basin, Zambia: upper Permian turnover and Middle-Upper Triassic vertebrate assemblages. *Journal of Vertebrate Paleontology, Programs and Abstracts, 2020*, 266.

RAY, S. 2000. Endothiodont dicynodonts from the Late Permian Kundaram Formation, India. *Palaeontology* **43**, 375–404.

RUBIDGE, B.S. 2005. Reuniting lost continents—fossil reptiles from the ancient Karoo and their wanderlust. *South African Journal of Geology* **108**, 135–172.

SEELEY, H.G. 1894. Researches on the structure, organisation, and classification of the fossil Reptilia.—Part IX., Section 1. On the Therosuchia. *Philosophical Transactions of the Royal Society of London, Series B, Biological Sciences* **185**, 987–1018.

SIDOR, C.A., TABOR, N.J. & SMITH, R.M.H. 2021. A new late Permian burnetiamorph from Zambia confirms exceptional levels of endemism in Burnetiamorpha (Therapsida: Biarmosuchia) and an updated paleoenvironmental interpretation of the Upper Madumabisa Mudstone Formation. *Frontiers in Ecology and Evolution* **9**, 685244.

SIDOR, C.A., ANGIELCZYK, K.D., WEIDE, D.M., SMITH, R.M.H., NESBITT, S.J. & TSUJI, L.A. 2010. Tetrapod fauna of the lowermost Usili Formation (Songea Group, Ruhuhu Basin) of southern Tanzania, with a new burnetiid record. *Journal of Vertebrate Paleontology* **30**, 696–703.

SIMÃO-OLIVEIRA, D. DE, KERBER, L. & PINHEIRO, F.L. 2020. Endocranial morphology of the Brazilian Permian dicynodont *Rastodon procurvidens* (Therapsida, Anomodontia). *Journal of Anatomy* **236**, 384–397.

SMITH, R.M.H. 2020. Biostratigraphy of the *Cistecephalus* Assemblage Zone (Beaufort Group, Karoo Supergroup), South Africa. *South African Journal of Geology* **123**, 181–190.

STRONG, E.E. & LIPSCOMB, D. 2000. Character coding and inapplicable data. *Cladistics* **15**, 363–371.

VAN HOEPEN, E.C.N. 1934. Oor die indeling van die Dicynodontoidae na aanleiding van nuwe vorme. *Paleontologiese Navorsing van die Nasionale Museum* **2**, 67–101.

VIGLIETTI, P.A. 2020. Biostratigraphy of the *Daptocephalus* Assemblage Zone (Beaufort Group, Karoo Supergroup), South Africa. *South African Journal of Geology* **123**, 191–206.

VIGLIETTI, P.A., ROJAS, A., ROSVALL, M., KLIMES, B. & ANGIELCZYK, K.D. 2022. Network-based biostratigraphy for the late Permian-mid Triassic Beaufort Group (Karoo Supergroup) in South Africa enhances biozone applicability and stratigraphic correlation. *Palaeontology* **65**, e12622.

WILD, R., KAAYA, C., KREUSER, T., MARKWORT, S. & SEMKIWA, P.Z. 1993. Discovery of a skull of *Dicynodon lacerticeps* in the uppermost Permian (Tatarian) of Tanzania. *Sonderveröffentlichungen, Geologisches Institut der Universität zu Köln* **70**, 231–242.

APPENDIX 1

Revised character state codings for *Compsodon helmoedi*, incorporating new data on mandibular morphology from NHCC LB211, and character state codings for the two species of *Emydops*. The character list and codings for all other taxa are the same as for the phylogenetic analysis of Angielczyk *et al*. (2021).

Discrete-state characters

Compsodon_helmoedi 1011101210 1000012010 0200111101 0101000010 0000211010 0000300211 002011?010 1110111031 1101012110 02000?0111 1200111111 01?1011200 4000202101 0011??1112 1????????? ?????????? ?????????? ?0??

Emydops_arctatus 1011101210 1000002000 0200111101 0101000000 0000101100 1000100201 0020111010 1111111030 1101012110 0210000011 1200101111 0101011(1 2)00 4000202101 0011311112 10?1?010?0 0000001110 ???0001211 ?00?

Emydops_oweni 1011?0?210 1000002000 02???11101 0101000000 0000101100 1000100?1 ?020111010 1111111030 ?101012110 12100?001? 1200101111 0??1011??0 4000202101 001??11?12 1????????? ?????????? ?????????? ????

Continuous characters

Compsodon_helmoedi 0.196 5.874 0.207 1.066 0.431 0.187 1.71 0.082 10.3 0.22 9.858 11.0 0.817 0.281 0.829 1.045 ? ? ? ? ? ? ?

Emydops_arctatus 0.221 5.871 0.204 0.904 0.541 0.165 1.626 0.119 9.85 0.174 9.7 8.936 0.85 0.385 0.669 0.967 0.668 0.428 0.23 0.454 1.283 0.0 0.353

Emydops_oweni 0.215 5.878 0.206 0.92 0.512 0.174 1.686 0.101 9.6 0.193 9.434 11.167 0.788 0.5 0.77 0.923 ? ? ? ? ? ? ?